Microstructure and electric response of Li,Sn co-doped NiO ceramics

Jiecheng Zeng, Tusheng He, Yang Liu*

School of Civil Engineering, Shaoguan University, Shaoguan 512005, China

Abstract

Phase composition, microstructure and electric response of $Li_{0.05}Sn_xNi_{0.95-x}O$ (x = 0, 0.025, 0.05, 0.1) ceramics were systematically investigated. Colossal dielectric permittivity (>5000) is observed in the frequency range of 10^2–10^5 Hz at room temperature which becomes highly frequency-independent with increasing temperature. Secondary Sn-rich phase is detected in the grain boundary regions and it has a remarkable influence on the dielectric properties. Impedance spectroscopy analysis demonstrates that the microstructure is electrically heterogeneous, consisting of semiconducting grain and insulating grain boundary. Defect dipoles or polyvalent cations induced at high temperature may activate an electron hopping process under electric field, resulting in the enhancements of grain conductivity and polarization effect. This behaviour should be considered as the origin of the observed dielectric response.

Keywords: grain boundaries, dielectric response, Maxwell-Wagner polarization, heterogeneous structure

I. Introduction

In past decade, NiO-based ceramics have attracted considerable attention for the potential application in electronic products such as memories and filters. Nan *et al.* [1] have firstly discovered giant dielectric constant (ε') and relative low dielectric loss ($\tan\delta$) near room temperature in (Li,Ti)-doped NiO ceramics. It was a new type of lead-free and non-ferroelectric oxides remaining high ε' in wide temperature and frequency ranges [1,2]. For (A,B) co-doped NiO ceramics, the dielectric properties can be tuned by varying the composition of additive A and B ions (A = Li, Na, K, Mg and B = Ti, Al, Si, Fe, V, Ta). Impedance spectroscopy analysis showed a heterogeneous microstructure consisting of semiconducting grains and insulating boundaries [1,3–8]. The origin of dielectric response is deem to be induced by a strong interfacial polarization at grain boundary layers. Free charge carriers start to move frequently under an applied electric field, and accumulate gradually at two sides of insulating grain boundaries regarding to the BLCs model [9]. However, Thongbai *et al.* [10] have found that the dielectric response is mainly attributed to two different mechanisms in whole frequency range: i) the space charge polarization at low frequency regions, and ii) the defect-dipole polarization at high frequency regions. Therefore, such explanation is still under discussion, and it is necessary to make a further study of it.

The rutile crystalline structural SnO_2 is seemingly a promising oxide to regulate the microstructure and electric properties of high dielectric materials. It can be inferred that small addition of SnO_2 to pure $BaTiO_3$ would produce well-defined grain boundaries [11]. In SnO_2 doped $CaCu_3Ti_4O_{12}$ ceramics, Sn^{4+} ions located at grain boundaries would make a dragging effect on the movement of grain boundary [12]. The changes at the grain boundary would influence the dielectric properties for the needs of the capacitors industry. In addition, both valences of Sn and Ti ions are tetravalent. The radius of Sn^{4+} (0.69 Å) is comparable to that of Ti^{4+} (0.61 Å), and more close to that of Ni^{2+} (0.69 Å). It is expected to investigate the effect of Sn doping on microstructure and dielectric response of NiO-based ceramics. In this paper, Li,Sn co-doped NiO ceramics was prepared successfully, and the dielectric properties were studied systematically. The results suggested that the microstructure was mainly heterogeneous. Sn doping had great impact on grain and grain boundary conductivity, and made major contributions to the electric response in these materials.

II. Experimental

$Li_{0.05}Sn_xNi_{0.95-x}O$ ceramics, where x = 0, 0.025,

---

*Corresponding authors: tel: +86 7518204209,
e-mail: *jackbotonliu@gmail.com*

0.05, 0.1), were prepared by a conventional solid-state reaction method. The samples with different Sn concentrations are referred to as LN, LSN1, LSN2 and LSN3, respectively. The purity of raw materials (Li_2CO_3, SnO_2 and NiO) was over 99.5%. The stoichiometric mixture of starting materials was ball-milled with ethyl alcohol for 10 h, and then calcined at 1000 °C for 5 h. The calcined dark green powders were ground and mixed with 4 wt.% solution of polyvinyl alcohol (PVA). The powders were pressed into discs with diameters of 10 mm and thickness of ~0.9 mm at 200 MPa. Finally, organic binder was burned out and the discs sintered at 1200–1350 °C for 5 h in air. After cooling to room temperature naturally, the surfaces of the discs were polished and coated with Ag electrodes, and fired at 550 °C for good ohmic contacts.

The phase compositions were investigated using a Bruker X-ray diffraction (CRD, Bruker D8 Advance). Microstructure and elemental analysis of the samples were performed using a scanning electron microscope (SEM) (QUANTAQ400, FEI) with energy dispersive spectroscopy (EDS). The relative density of the samples was measured and calculated by Archimedes method with distilled water as an immersion medium. Impedance analysis and dielectric properties were measured using WK6500 LCR Meter in frequency range from 100 Hz to 1 MHz with oscillation voltage of 1.0 V. The measurements were carried out at temperatures ranging from −80 to 350 °C. Valence states of cations were characterized using X-ray photoelectron spectroscopy (Thermo ESCALAB250XI).

III. Results and discussion

XRD patterns of $Li_{0.05}Sn_xNi_{0.95-x}O$ (x = 0, 0.025, 0.05, 0.1) ceramics sintered at 1350 °C for 5 h are presented in Fig. 1. Diffraction peaks are mainly indexed to cubic NiO phase in space group $Fm\bar{3}m$ (JCPDS 78-0429). It shows main peaks at 37.3°, 43.3°, 62.9°, 75.4° and 79.4° corresponding to the (111), (200), (220), (311) and (222) planes, respectively. No other phase peak was detected in LN ceramics, indicating that Li^+ has successfully substituted Ni^{2+} site. The lattice parameters of the LN, LSN1, LSN2 and LSN3 samples were estimated using Cohen's least mean square method to be 4.178, 4.176, 4.180 and 4.171 Å, respectively, which were comparable to that of NiO (4.177 Å). Secondary SnO_2 phase was observed obviously in Li,Sn doped NiO
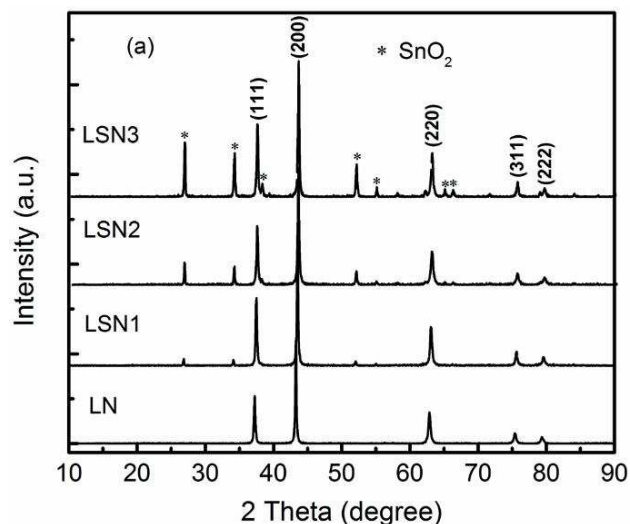

Figure 1. XRD patterns for $Li_{0.05}Sn_xNi_{0.95-x}O$ (x = 0, 0.025, 0.05, 0.1) ceramics sintered at 1350 °C for 5 h

ceramics. The relative intensity ratio of SnO_2 peaks, in particular, was enhanced gradually with increasing Sn concentration. Despite the same ionic radius of Sn^{4+} and Ni^{2+} (0.69 Å), the charge difference between Ni^{2+} and Sn^{4+} is large. This makes it difficult to form the solid solution, indicating the presence of separate SnO_2 grains.

Figure 2 shows SEM images of $Li_{0.05}Sn_xNi_{0.95-x}O$ (x = 0, 0.025, 0.05, 0.1) ceramics sintered at 1350 °C for 5 h. SEM images of the LSN2 sintered at 1200–1350 °C for 5 h are presented in Fig. 3. The mean grain sizes and relative densities were listed in Table 1. It can be seen that grain size as well as density increases with increasing sintering temperature. The microstructure is heterogeneous and consists of many large grains separated by small grains. Figure 4 displays the results of the regional elemental mapping of the LSN3 ceramics. The elements Sn, Ni and O were captured, and no Li was detected because of its lower atomic mass [13]. According to the distribution of each element, the large grains refer to NiO while the small grains represent SnO_2. Moreover, it is worthy to note that separated Sn-rich phase becomes enriched with the increase of Sn concentration. That may prevent the diffusion of grain boundary and suppress the growth of grain.

Figure 5 shows the frequency dependence of dielectric behaviour for $Li_{0.05}Sn_xNi_{0.95-x}O$ (x = 0, 0.025, 0.05, 0.1) ceramics at room temperature. ε' is over 5000, and nearly stable in the frequency range of 10^2–10^5 Hz.

Table 1. Physical properties of $Li_{0.05}Sn_xNi_{0.95-x}O$ (x = 0, 0.025, 0.05, 0.1) ceramics sintered at different temperatures

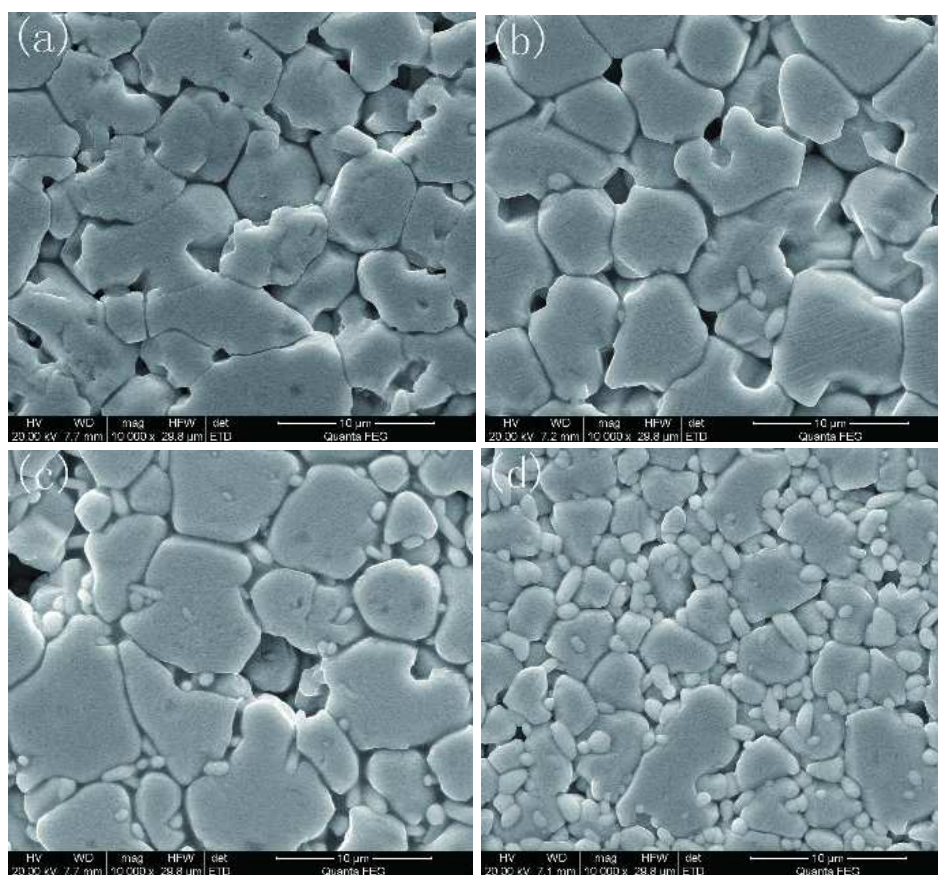| Sample	Sintering condition	Mean grain size [μm]	Relative density [%]
$Li_{0.05}Ni_{0.95}O$	1350 °C/5 h	5.12	87.0
$Li_{0.05}Sn_{0.025}Ni_{0.925}O$	1350 °C/5 h	5.68	89.1
$Li_{0.05}Sn_{0.05}Ni_{0.90}O$	1200 °C/5 h	2.13	82.4
$Li_{0.05}Sn_{0.05}Ni_{0.90}O$	1250 °C/5 h	3.98	88.5
$Li_{0.05}Sn_{0.05}Ni_{0.90}O$	1300 °C/5 h	5.04	90.3
$Li_{0.05}Sn_{0.05}Ni_{0.90}O$	1350 °C/5 h	5.86	91.5
$Li_{0.05}Sn_{0.10}Ni_{0.85}O$	1350 °C/5 h	4.87	91.6

Figure 2. SEM images for $Li_{0.05}Sn_xNi_{0.95-x}O$ ($x = 0$, 0.025, 0.05, 0.1) ceramics sintered at 1350 °C for 5 h

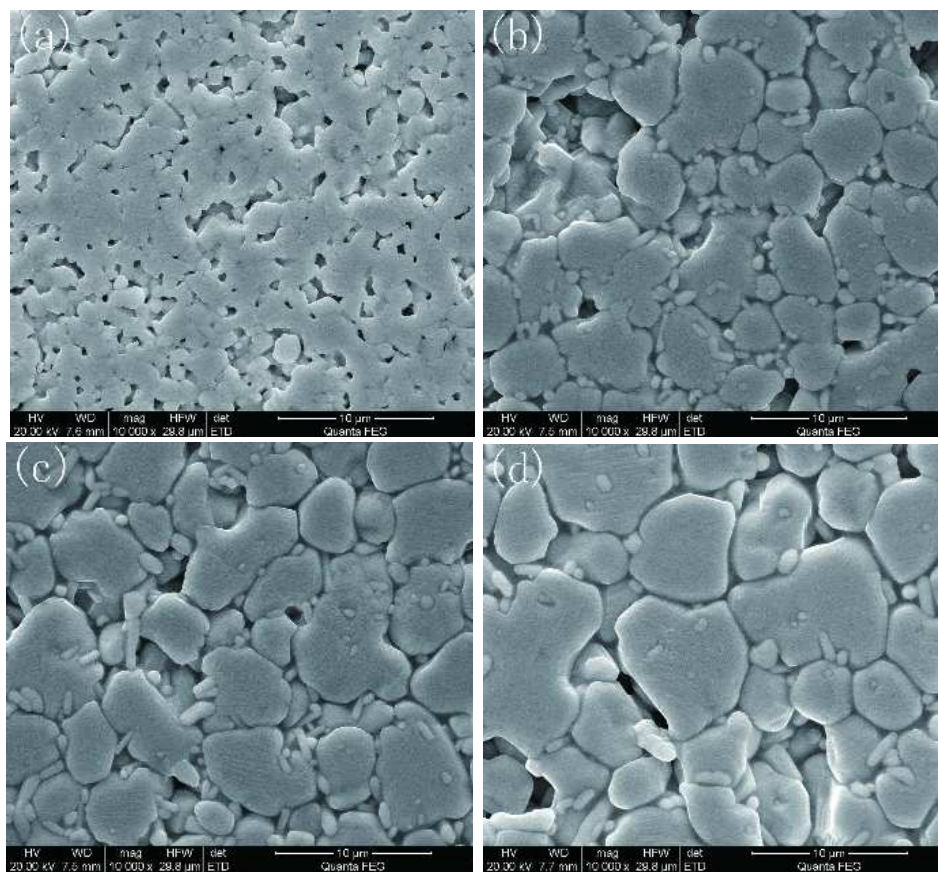**Figure 3. SEM images for $Li_{0.05}Sn_{0.05}Ni_{0.90}O$ ceramics sintered at 1200–1350 °C for 5 h**
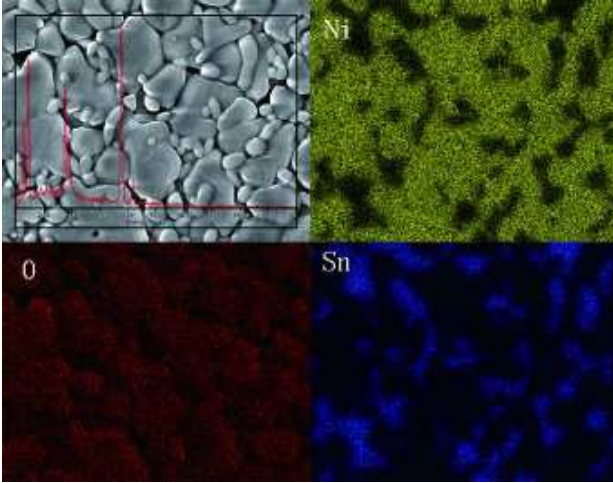
Figure 4. Elemental mapping of Li$_{0.05}$Sn$_{0.10}$Ni$_{0.85}$O ceramics sintered at 1350 °C for 5 h

Figure 7. Arrhenius plots of relaxation time for Li$_{0.05}$Sn$_x$Ni$_{0.95-x}$O (x = 0.025, 0.05, 0.1) ceramics sintered at 1350 °C for 5 h
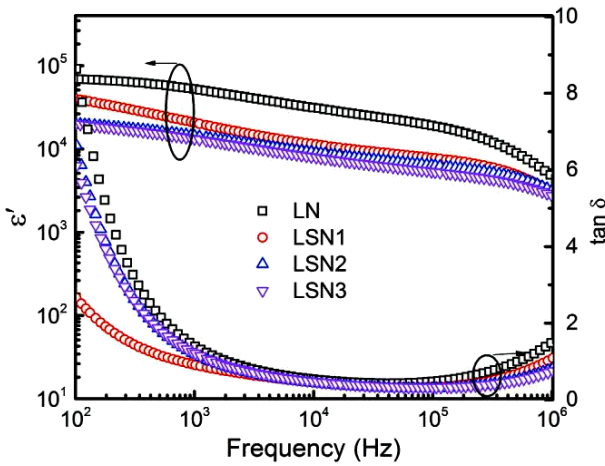
Figure 5. Frequency dependence of ε' and tan δ of Li$_{0.05}$Sn$_x$Ni$_{0.95-x}$O (x = 0, 0.025, 0.05, 0.1) ceramics at room temperature
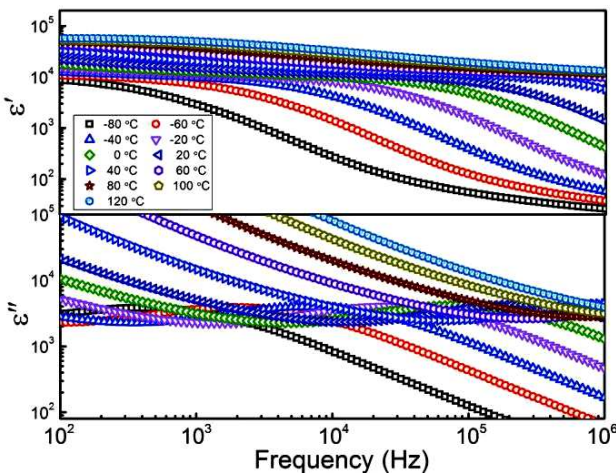
Figure 6. Frequency dependence of ε' and ε'' at different temperatures for Li$_{0.05}$Sn$_{0.05}$Ni$_{0.90}$O ceramics

Meanwhile, ε' visibly decreases with increasing Sn concentration. The values of tan δ of the LN, LSN1, LSN2 and LSN3 ceramics at room temperature and 50 kHz
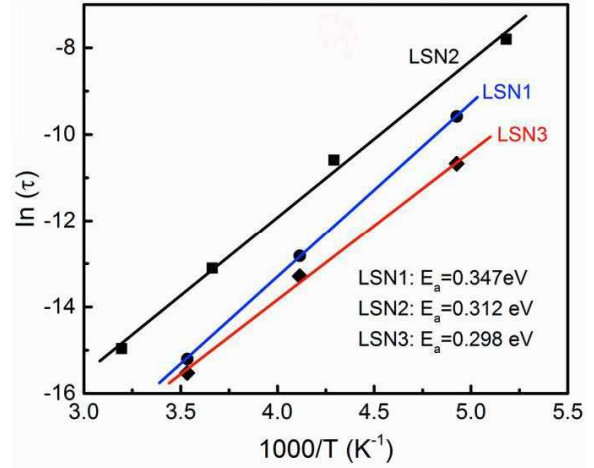
were approximately 0.434, 0.324, 0.303 and 0.298, respectively, indicating that tan δ decreases with Sn doping significantly. Figure 6 illustrates the frequency dependence of dielectric response at various measured temperatures for the LSN2 ceramics sintered at 1350 °C. Colossal ε' values are exhibited over the frequency range of 10^2–10^5 Hz above 40 °C, which is about three orders of magnitude higher than that of the pure NiO ceramics [14]. A typical step-like decrease in ε' was observed at high frequency, indicating a Debye-type relaxation occurring [1]. Furthermore, ε' strongly depends on frequency at low temperature. As the measured temperature increases, the value of ε' visibly increases and becomes more frequency-independent. The dielectric relaxation peak of ε'' was observed and gradually shifted to higher frequencies with increasing temperature. This dielectric behaviour can be ascribed to the Maxwell-Wagner effect corresponding to a step-like decrease in ε' [15–17]. On the basis of the BLCs model, the low-frequency response of colossal permittivity dielectrics is attributed to the interface polarization. On the other hand, the electric properties of grain boundary should be a main factor at intermediate-frequency, while at the high-frequency they may be originated from the bulk [18]. Generally, polarization effect of NiO-based materials is produced and enhanced by increasing temperature, revealing a thermal-activated relaxation. Figure 7 demonstrates the relationships between ln(τ) and $1000/T$ for the LSN1, LSN2 and LSN3 ceramics. These plots are best fitting line following the Arrhenius law:

$$\tau = \tau_0 \exp \frac{E_0}{k_B \cdot T} \tag{1}$$

where E_a is the activation energy and k_B is the Boltzmann constant. The values of E_a for the LSN1, LSN2 and LSN3 were calculated to be 0.347, 0.312 and 0.298 eV, respectively, which is comparable to the values of 0.126–0.483 eV for those reported for NiO-based ceramics [4,7,10].
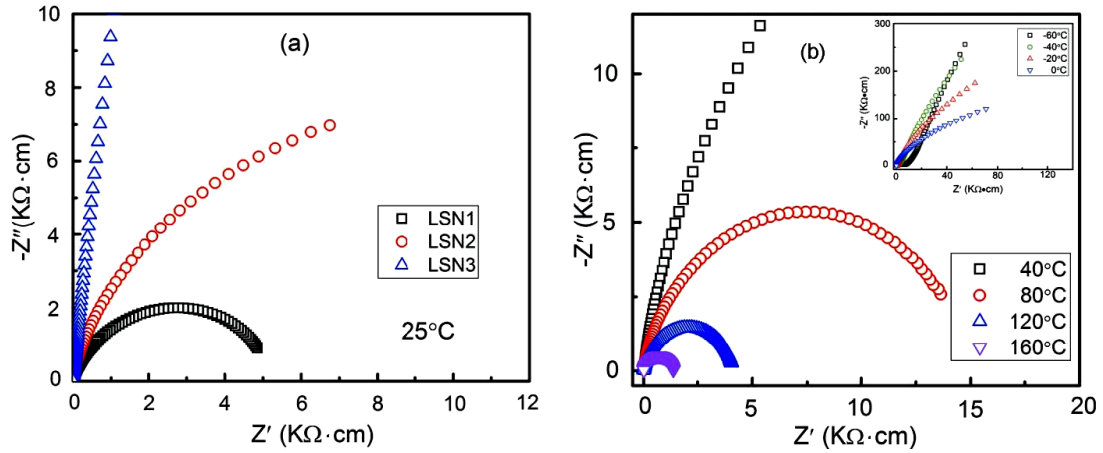
Figure 8. Impedance complex plane plot for: a) Li$_{0.05}$Sn$_x$Ni$_{0.95-x}$O (x = 0.025, 0.05, 0.1) ceramics sintered at 1350 °C for 5 h and b) Li$_{0.05}$Sn$_{0.05}$Ni$_{0.90}$O ceramics at selected temperatures
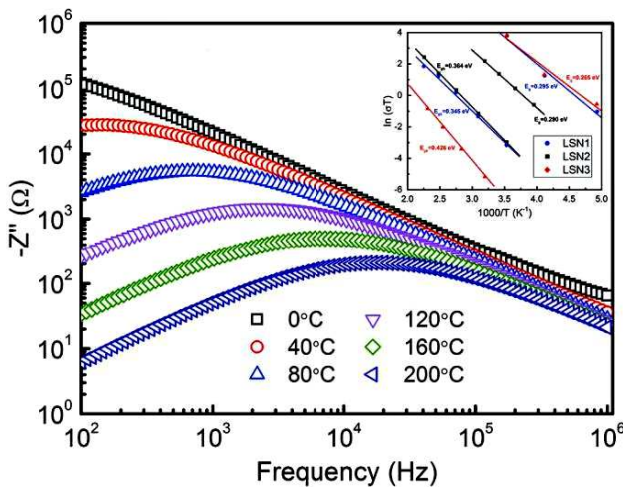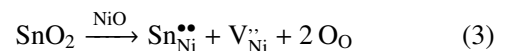

Figure 9. Frequency dependence of Z'' at different temperatures for Li$_{0.05}$Sn$_{0.05}$Ni$_{0.90}$O ceramics (inset shows Arrhenius plot of E_g and E_{gb} for Li$_{0.05}$Sn$_x$Ni$_{0.95-x}$O where x = 0.025, 0.05, 0.1)

The impedance spectroscopy measurement is widely used to better understand the characteristics of electric response in dielectrics, especially caused by bulk and grain boundary. An equivalent circuit model containing two parallel RC elements (R_gC_g and $R_{gb}C_{gb}$) has been introduced. The element R_gC_g at high frequencies describes the semiconducting grains, while the element $R_{gb}C_{gb}$ at low frequencies delineates the insulating grain boundaries [19]. Figure 8a shows the impedance complex plane plot for the LSN1, LSN2 and LSN3 samples at room temperature. It can be seen that the addition of Sn has a great influence on the grain boundary resistivity (R_{gb}). The R_{gb} increases with increasing Sn concentration, which may be associated with the secondary SnO$_2$ gathered at the grain boundary regions. Figure 8b and inset show impedance complex plane plot at high and low temperatures for the LSN2 sample, respectively. The R_g and R_{gb} decrease with increasing temperatures overall, and the value of R_g is much smaller than that of R_{gb}. This manifests a heterogeneous structure consisting of semiconducting grains and insulating grain bound-

aries. According to the EDS result, Sn-rich phase was accumulated at the grain boundaries to form an insulating barrier, implying the origin of differences on electrical properties of grain and grain boundary. It should be responsible for the colossal dielectric response of the Li,Sn co-doped NiO ceramics [7].

Figure 9 demonstrates the frequency dependence of Z'' at different temperatures for the LSN2 sample. Z'' peak corresponding to a thermally-activated electric response at low frequency was observed. As temperature increases, the peak position shifts to higher frequency ranges, and the peak height decreases. It is ascribed to the effect of grain boundary [20,21]. Inset in Fig. 9 shows the Arrhenius plots of conduction and activation energies of grain (E_g) and grain boundary (E_{gb}). The values of E_g were 0.295, 0.290 and 0.265 eV and of E_{gb} were 0.345, 0.364 and 0.426 eV for the LSN1, LSN2 and LSN3, respectively. It is significant that the conduction activation energy of grain is smaller than that of grain boundary, confirming the different electrical transport mechanisms for grain and grain boundary.

NiO is a Mott-Hubbard insulator at room temperature [22]. However, introduction of monovalent or other valence state cations leads to an increase in the conductivity of NiO [15]. Figure 10 illustrates the XPS analysis of Ni2p$_{3/2}$ peak of the LSN2 ceramics. The Ni2p$_{3/2}$ peak region is divided into two peaks ascribed to the contribution from Ni^{2+} and Ni^{3+}. Monovalent cations doping such as Li$^+$ or Na$^+$ ion doping may cause the transformation of Ni^{2+} adjacent into Ni^{3+} to keep charge neutrality [1,15,23]. In addition, some crystallographic distortions are induced because of the comparable radius of Li$^+$, Sn^{4+} and Ni^{2+} ions. More importantly, defects can be introduced to the sample due to the different valences of ions as follows:

$$\text{Li}_2\text{O} \xrightarrow{\text{NiO}} 2\,\text{Li}_{\text{Ni}}' + \text{V}_\text{O}^{\bullet\bullet} + \text{O}_\text{O} \qquad (2)$$

$$\text{SnO}_2 \xrightarrow{\text{NiO}} \text{Sn}_{\text{Ni}}^{\bullet\bullet} + \text{V}_{\text{Ni}}'' + 2\,\text{O}_\text{O} \qquad (3)$$

According to the EDS observation, $\text{V}_\text{O}^{\bullet\bullet}$ might be generated in the grain while V_{Ni}'' might be responsible for
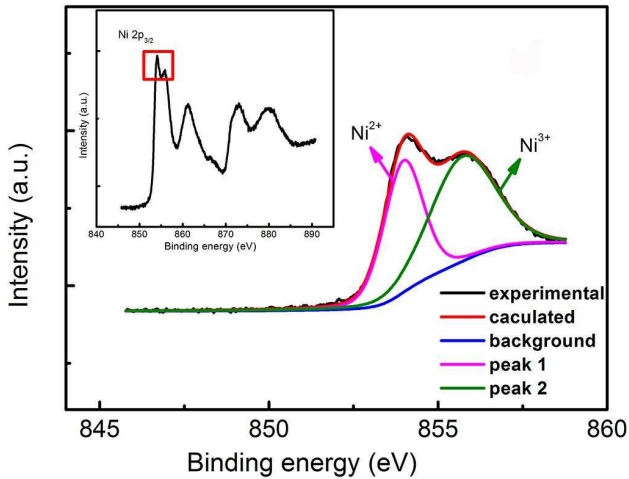
Figure 10. XPS spectrum of Ni2p$_{3/2}$ peak of Li$_{0.05}$Sn$_{0.05}$Ni$_{0.90}$O ceramics
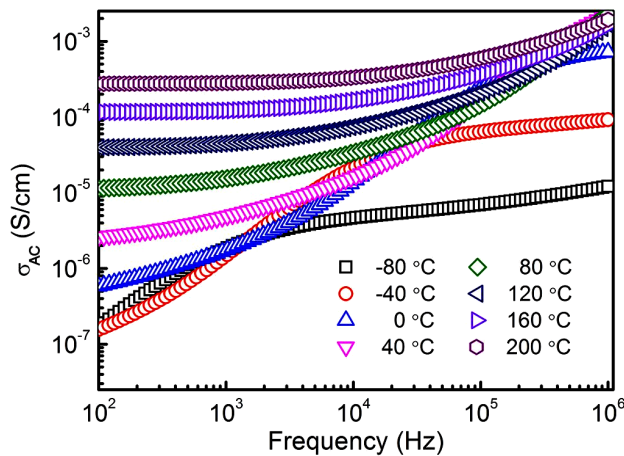

Figure 11. Frequency dependence of σ_{AC} at different temperatures for Li$_{0.05}$Sn$_{0.05}$Ni$_{0.90}$O ceramics

the insulation of the grain boundary. Thus, the defect dipoles ($V_O^{\bullet\bullet} - 2\,Li_{Ni}'$) and polyvalent cations (Ni^{2+} and Ni^{3+}) may enhance the conductivity of the grain, and partially influence dielectric permittivity of the Li,Sn co-doped NiO samples.

Figure 11 shows the temperature dependence of AC conductance (σ_{AC}) of the LSN2 ceramics in the frequency range from 10^2 to 10^6 Hz. In general, the AC conductance is often expressed according to the AC power law [24]:

$$\sigma_{AC} = \sigma_{DC} + A \cdot f^n \qquad (4)$$

where σ_{DC} is the DC conductance and $A \cdot f^n$ is the frequency-dependent component. At sufficiently low frequencies, σ_{AC} is dominated by σ_{DC}, which is independent of frequency, but strongly temperature-dependent. As frequency increases, σ_{AC} is dominated by the component $A \cdot f^n$ gradually. This is because σ_{AC} originates from the hopping conduction process [25–27]. Since temperature is sufficiently low, hopping is not active, and electric field does not influence the hopping

conduction. As temperature increases, electron hopping starts, more charge carriers are produced (e.g. $V_O^{\bullet\bullet}$ and Ni^{3+}) and the polarization effect enhances. The applied electric field begins to influence the hopping process with increasing frequency. This improves charge carriers' drift mobility, and long range motion does not occur. Thus, the value of σ_{AC} increases moderately.

IV. Conclusions

A series of Li,Sn co-doped NiO ceramics was fabricated by a conventional solid-state reaction method. Phase composition, microstructure and electric response were studied systematically. Impedance analysis demonstrated an electrically heterogeneous microstructure. Secondary Sn-rich phase was accumulated at the grain boundaries to form an insulating barrier, indicating the different conduction mechanism of grain and grain boundary. Colossal ε' of over 10^4 was obtained at high temperatures which became highly frequency-independent. Polyvalent cations or defect dipoles partially influence the conductivity inside the grains, and result in colossal dielectric properties.

References

1. J. Wu, C.W. Nan, Y. Lin, Y. Deng, "Giant dielectric permittivity observed in Li and Ti doped NiO", *Phys. Rev. Lett.*, **89** (2002) 217601.
2. Y.H. Lin, M. Li, C.W. Nan, J. Li, J. Wu, J. He, "Grain and grain boundary effects in high-permittivity dielectric NiO-based ceramics", *Appl. Phys. Lett.*, **89** (2006) 032907.
3. Y. Lin, J. Wang, L. Jiang, Y. Chen, C.W. Nan, "High permittivity Li and Al doped NiO ceramics", *Appl. Phys. Lett.*, **85** (2004) 5664–5666.
4. Y. Lin, L. Jiang, R. Zhao, C.W. Nan, "High permittivity core/shell structured NiO-based ceramics and their dielectric response mechanism", *Phys. Rev. B*, **72** (2005) 014103.
5. P. Thongbai, T. Yamwong, S. Maensiri, "Electrical responses in high permittivity dielectric (Li,Fe)-doped NiO ceramics", *Appl. Phys. Lett.*, **94** [15] (2009) 152905.
6. P.K. Jana, S. Sarkar, H. Sakata, T. Watanabe, B.K. Chaudhuri, "Microstructure and dielectric properties of Na$_x$Ti$_y$Ni$_{1-x-y}$O (x = 0.05-0.30, y = 0.02)", *J. Phys. D: Appl. Phys.*, **41** [6] (2008) 065403.
7. Y.J. Hsiao, Y.S. Chang, T.H. Fang, Y.L. Chai, C.Y. Chung, "High dielectric permittivity of Li and Ta codoped NiO ceramics", *J. Phys. D: Appl. Phys.*, **40** [3] (2007) 863–868.
8. B. Cheng, Y.H. Lin, J.N. Cai, C.W. Nan, "Preparation of Mg and Ti co-doped NiO-based ceramic and its high dielectric properties", *Key Eng. Mater.*, **368** (2008) 37–39.
9. A.A. Dakhel, "Giant dielectric permittivity in Li and Pr co-doped NiO ceramics", *J. Alloys Comp.*, **488** [1] (2009) 31–34.
10. P. Thongbai, S. Tangwancharoen, T. Yamwong, S. Maen-

siri, "Dielectric relaxation and dielectric response mechanism in (Li, Ti)-doped NiO ceramics", *J. Phys.: Condens. Matter*, **20** (2008) 395227.

11. Z.H. Dughaish, "Dielectric properties of $(BaTiO_3)_{(1-x)}(SnO_2)_x$ ceramics", *J. Nat. Sci. Math.*, **6** [2] (2013) 107–121.

12. H. Xiang, Z. Chen, D. Liu, H. Dai, T. Li, W. Zhang, "Microstructure and dielectric properties of SnO_2-doped $CaCu_3Ti_4O_{12}$ ceramics", *Ferroelectrics*, **474** [1] (2015) 43–53.

13. Z. Li, C. Wang, X. Ma, L. Yuan, J. Sun, "Synthesis, structures and electrochemical properties of $Li_xNi_{1-x}O$", *Mater. Chem. Phys.*, **91** [1] (2005) 36–39.

14. Y. Lin, R. Zhao, J. Wang, J. Cai, C.W. Nan, Y. Wang, L. Wei, "Polarization of high-permittivity dielectric NiO-based ceramics", *J. Am. Ceram. Soc.*, **88** [7] (2005) 1808–1811.

15. Y.J. Li, X.M. Chen, R.Z. Hou, Y.H. Tang, "Maxwell-Wagner characterization of dielectric relaxation in $Ni_{0.8}Zn_{0.2}Fe_2O_4/Sr_{0.5}Ba_{0.5}Nb_2O_6$ composite", *Solid State Commun.*, **137** [3] (2006) 120–125.

16. Y. Zhi, A. Chen, "Maxwell-Wagner polarization in ceramic composites $BaTiO_3$-$(Ni_{0.3}Zn_{0.7})Fe_{2.1}O_4$", *J. Appl. Phys.*, **91** [2] (2002) 794–797.

17. R. Waser, R. Hagenbeck, "Grain boundaries in dielectric and mixed-conducting ceramics", *Acta Mater.*, **48** [4] (2000) 797–825.

18. R. Schmidt, M.C. Stennett, N.C. Hyatt, J. Pokorny, J. Prado-Gonjal, M. Li, D.C. Sinclair, "Effects of sintering temperature on the internal barrier layer capacitor (IBLC) structure in $CaCu_3Ti_4O_{12}$ (CCTO)", *J. Eur. Ceram. Soc.*, **32** [12] (2012) 3313–3323.

19. M. Li, Z. Shen, M. Nygren, A. Feteira, D.C. Sinclair, A.R. West, "Origin(s) of the apparent high permittivity in $CaCu_3Ti_4O_{12}$ ceramics: clarification on the contributions from internal barrier layer capacitor and sample-electrode contact effects", *J. Appl. Phys.*, **106** [10] (2009) 104106.

20. T.B. Adams, D.C. Sinclair, A.R. West, "Giant barrier layer capacitance effects in $CaCu_3Ti_4O_{12}$ ceramics", *Adv. Mater.*, **14** [18] (2002) 1321–1323.

21. D.C. Sinclair, T.B. Adams, F.D. Morrison, A.R. West, "$CaCu_3Ti_4O_{12}$: One-step internal barrier layer capacitor", *Appl. Phys. Lett.*, **80** [12] (2002) 2153–2155.

22. Y. Nakamura, H. Ogawa, T. Nakashima, A. Kishimoto, H. Yanagida, "Strain-dependent electrical conduction in the system NiO-CaO", *J. Am. Ceram. Soc.*, **80** [6] (1997) 1609–1611.

23. H.M. Kotb, M.M Ahmad, N.A. Alraheem, "Study of the structural, impedance spectroscopy and dielectric properties of Na and Si co-doped NiO ceramics", *J. Phys. D: Appl. Phys.*, **50** [43] (2017) 435304.

24. S. Manna, S.K. De, "Giant dielectric permittivity observed in Li and Zr co-doped NiO", *Solid State Commun.*, **150** [9] (2010) 399–404.

25. R.M. Hill, A.K. Jonscher, "DC and AC conductivity in hopping electronic systems", *J. Non-Cryst. Solids*, **32** [1-3] (1979) 53–69.

26. K. Raman, O.P. Thakur, R.P. Tandon, "Study of structural, dielectric and electrical conduction behaviour of Gd substituted $CaCu_3Ti_4O_{12}$ ceramics", *Ceram. Int.*, **38** [4] (2012) 3029–3037.

27. Y. Liu, X. Zhao, "Dielectric properties and impedance characteristics of BaO-Cr_2O_3-Sb_2O_5 ceramics", *J. Mater. Sci.: Mater. Electron.*, **26** [9] (2015) 6712–6717.